The physiological cargo adaptor of kinesin-2 functions as an evolutionary conserved lockpick

Augustine Cleetus[a,1], Georg Merck[a,1], Felix Mueller-Planitz[b,2], and Zeynep Ökten[a,2]

Edited by Trina Schroer, The Johns Hopkins University, Baltimore, MD; received June 2, 2021; accepted June 22, 2022 by Editorial Board Member Rebecca Heald

Specific recognition of cellular cargo and efficient transport to its correct intracellular destination is an infrastructural challenge faced by most eukaryotic cells. This remarkable deed is accomplished by processive motor proteins that are subject to robust regulatory mechanisms. The first level of regulation entails the ability of the motor to suppress its own activity. This autoinhibition is eventually relieved by specific cargo binding. To better understand the role of the cargo during motor activation, we dissected the activation mechanism of the ciliary homodimeric kinesin-2 from *Caenorhabditis elegans* by its physiological cargo. In functional reconstitution assays, we identified two cargo adaptor proteins that together are necessary and sufficient to allosterically activate the autoinhibited motor. Surprisingly, the orthologous adaptor proteins from the unicellular green algae *Chlamydomonas reinhardtii* also fully activated the kinesin-2 from worm, even though *C. reinhardtii* itself lacks a homodimeric kinesin-2 motor. The latter suggested that a motor activation mechanism similar to the *C. elegans* model existed already well before metazoans evolved, and prompted us to scrutinize predicted homodimeric kinesin-2 orthologs in other evolutionarily distant eukaryotes. We show that the ciliate *Tetrahymena thermophila* not only possesses a homodimeric kinesin-2 but that it also shares the same allosteric activation mechanism that we delineated in the *C. elegans* model. Our results point to a much more fundamental role of homodimeric kinesin-2 in intraflagellar transport (IFT) than previously thought and warrant further scrutiny of distantly related organisms toward a comprehensive picture of the IFT process and its evolution.

kinesin-2 | intraflagellar transport | evolution | regulation

Significance

The use of the homodimeric kinesin-2 in ciliogenesis has so far been demonstrated conclusively in the *Caenorhabditis elegans* model only. In this work, we uncover an activation mechanism of the homodimeric kinesin-2 that is shared between the multicellular animal *C. elegans* and the ciliate *Tetrahymena thermophila*. We identify two strictly conserved cargo adaptors that are necessary and sufficient to allosterically activate the respective motors. Notably, adaptors from the distantly related unicellular and mammalian models function as a 'lockpick' to fully unleash the activity of the worm kinesin-2 motor, suggesting that this activation mechanism is ancient and likely applies to more organisms given the conservation of the adaptors. Therefore, homodimeric kinesin-2 may play more fundamental roles in ciliogenesis than previously recognized.

Almost all eukaryotic cells deploy numerous different myosins, kinesins, and dyneins to transport an astonishingly diverse set of intracellular cargo on the actin and microtubule cytoskeleton. These motor proteins appear to know when to be active or inactive, and which particular cargo to transport among many. Unmasking the molecular mechanisms of how motor proteins recognize their designated cargo, and how they are switched on and off at the right time and place is therefore a prerequisite to understand the intricacies of intracellular transport.

One particularly strict regulation of motor behavior is observed during the intraflagellar transport (IFT) that is essential for the construction of virtually all eukaryotic cilia or flagella (1–3). IFT is driven by the oppositely directed kinesin-2 and dynein-2 motors that are activated reciprocally between the ciliary base and the tip, respectively (4). While all ciliated eukaryotes studied so far deploy a dynein-2 for the retrograde transport of the IFT trains from the ciliary tip to the base, the use of kinesin-2 motors for the transport from the ciliary base to the tip differs considerably between species. For example, the green algae *Chlamydomonas reinhardtii* builds its flagella with the heterotrimeric *Cr*FLA8/10/KAP kinesin-II motor (*SI Appendix*, Fig. S1, *Top*, see Table S1*A* for an overview of kinesin-2 motors and their oligomerization properties) (5–8). The multicellular animal *Caenorhabditis elegans* deploys a homodimeric *Ce*OSM-3 kinesin-2, in addition to the heterotrimeric kinesin-II, to build its cilia (*SI Appendix*, Fig. S1, *Middle*) (9). Curiously, even though the mouse ortholog of the *Ce*OSM-3 motor, the *Mm*KIF17 kinesin-2, is also found in the cilium, it does not function as an IFT motor (10–13). Instead, *Mm*KIF17 behaves as an inactive passenger on the IFT trains (*SI Appendix*, Fig. S1, *Bottom*). Molecular mechanisms that give rise to these species-specific differences in kinesin-2 regulation remain unknown.

Despite their divergent behavior in vivo, however, it is clear that the respective kinesin-2 orthologs from *C. elegans* (*Ce*OSM-3) and mouse (*Mm*KIF17) are both autoinhibited, i.e., they can suppress their own adenosine triphosphatase (ATPase) activity and switch themselves off (14, 15). Such self-regulatory mechanisms in fact apply to several myosins and dyneins as well (4, 16–18). Autoinhibition is thought to prevent

Author contributions: A.C., G.M., and Z.Ö. designed research; A.C. and G.M. performed research; A.C., G.M., and F.M.-P. analyzed data; and A.C., G.M., and Z.Ö. wrote the paper.

The authors declare no competing interest.

This article is a PNAS Direct Submission. T.A.S. is a Guest Editor invited by the Editorial Board.

[1]A.C. and G.M. contributed equally to this work.

[2]To whom correspondence may be addressed. Email: zoekten@ph.tum.de or felix.mueller-planitz@tu-dresden.de.

This article contains supporting information online at http://www.pnas.org/lookup/suppl/doi:10.1073/pnas.2109378119/-/DCSupplemental.

Published August 10, 2022.

futile adenosine triphosphate (ATP) hydrolysis if the motor is not bound to any intracellular cargo and cargo-binding eventually relieves the autoinhibition to enable active transport of cargo by the motor protein (17, 19). In most cases, recruitment of a motor to its designated cargo is mediated by an adaptor protein (20–23). In the case of the *Ce*OSM-3 kinesin-2, it is the evolutionary conserved adaptor protein DYF-1/IFT70 (*Ce*IFT70 hereafter, see *SI Appendix*, Table S1*B* for the species-specific nomenclature and the respective orthologs of the adaptors used in this study) that specifically recruits and activates the autoinhibited motor for directional transport in vivo and in vitro (Fig. 1*A*) (24, 25). The latter thus provokes the question why the mammalian *Mm*KIF17 kinesin-2 remains inactive despite the presence of *Mm*IFT70 in the cilium (*SI Appendix*, Fig. S1, *Bottom* and Table S1*B*) (11, 26). However, the knowledge of homodimeric kinesin-2 motors is limited as they have been mechanistically characterized in the *C. elegans* and mouse models only (14, 15, 25).

While it is clear that specific motor recruitment to a given cargo and motor activation represent key steps of regulated intracellular transport, the molecular details of motor-cargo interaction and how such interaction gives rise to the activation of the motor protein remain largely unknown. Scarcity of reconstituted motor-cargo complexes is arguably one of the major obstacles on the way toward a molecular picture of how cells regulate the transport of intracellular cargo. Here we turned to the first reconstituted kinesin-2-cargo complex to dissect the cargo-mediated motor activation mechanism as a physiologically relevant example.

Results and Discussion

The Distal C Terminus is Involved in the Autoinhibition of *Ce*OSM-3. Kinesins dimerize with their coiled-coil domain (or stalk) of varying lengths followed by a random coil domain (or tail domain) at the distal C terminus (Fig. 1*B*). Both, the stalk and the tail domains have been implicated in the autoinhibition of kinesin motors (14, 27, 28). Autoinhibition is thought to take place through intramolecular folding that puts the N-terminal catalytic head domain in direct contact to the distal tail domains

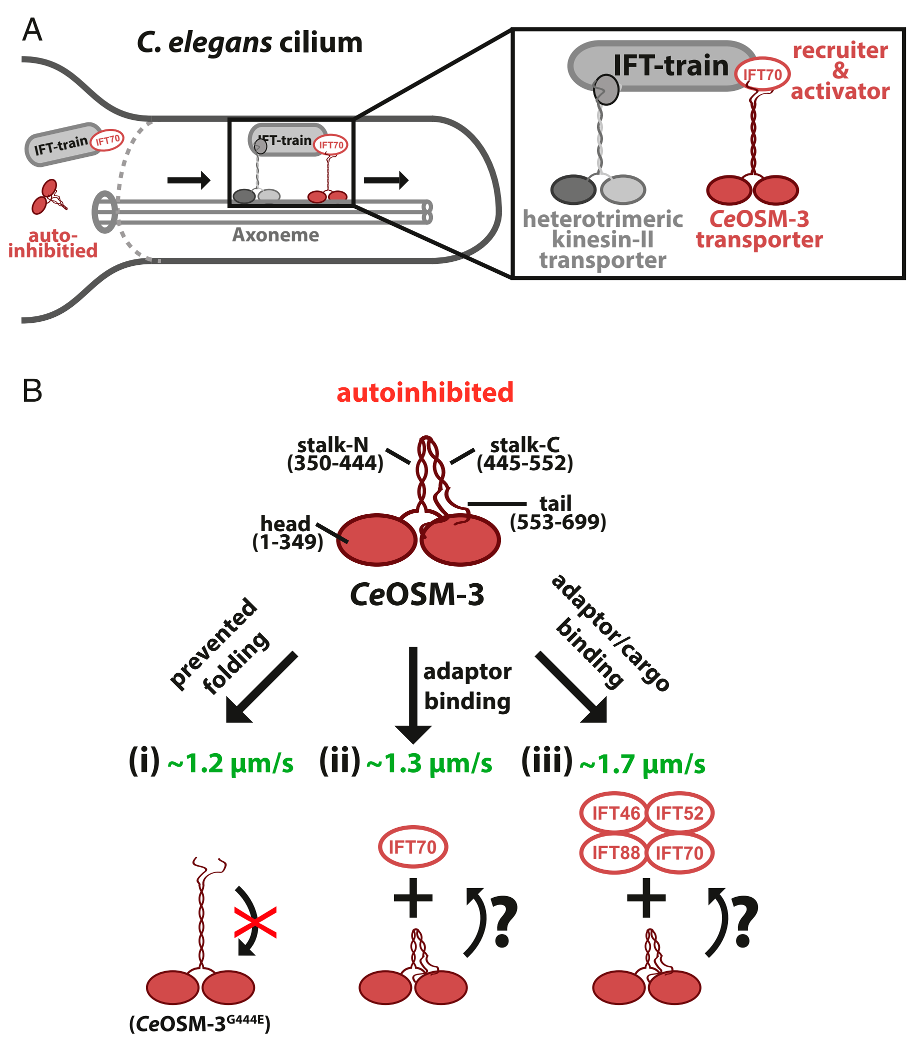

Fig. 1. Activation mechanism of *Ce*OSM-3. (*A*) To power its IFT trains toward the ciliary tip, *C. elegans* deploys a heterotrimeric kinesin-II and a homodimeric *Ce*OSM-3 kinesin-2 motor (*C. elegans* components are color-coded in red hereafter). At the ciliary base, the autoinhibited *Ce*OSM-3 must be recruited to the IFT trains and activated for anterograde transport. Here, the *Ce*IFT70 adaptor plays a key role in the specific recruitment and activation of the *Ce*OSM-3 kinesin-2. (*B*) Proposed models of autoinhibition and activation of the *Ce*OSM-3 motor. The distal C-terminal tail (553-699) folds onto the N-terminal head domains (1-349) to inhibit the motor's enzymatic activity. This autoinhibitory folding is mediated by the conserved glycine (G444) that is found roughly in the middle of the coiled-coil stalks (350-552) (see *SI Appendix*, Fig. S2). (*i*) The autoinhibition can be relieved by mutating the flexible glycine into a glutamic acid residue (*Ce*OSM-3^{G444E}). Preventing folding of the tail onto the head domains results in a constitutively activated motor with a velocity of ∼1.1 to 1.2 µm/s (15, 25). (*ii*) The same activation is achieved when the autoinhibited *Ce*OSM-3 motor binds to its *Ce*IFT70 adaptor subunit (25). (*iii*) The *Ce*IFT70-mediated incorporation of the autoinhibited *Ce*OSM-3 into its cargo complex (*Ce*IFT70/52/46/88), significantly increases the motor's speed to ∼1.7 µm/s (25).

(Fig. 1*B*) (27, 29, 30). Consistent with this notion, preventing intramolecular folding through mutation of the flexible glycine residue through a point mutation (*Ce*OSM-3^{G444E}) sufficed to partially activate the autoinhibited *Ce*OSM-3 kinesin-2 from *C. elegans* (15), and the motor could now move with ∼1.1 to 1.2 µm/s on surface-attached microtubules (Fig. 1*B*, *i*) (15, 25). A similar result was obtained by binding the autoinhibited *Ce*OSM-3 to its specific *Ce*IFT70 adaptor protein (Fig. 1*B*, *ii*) (25). Of note, when the *Ce*OSM-3/*Ce*IFT70 complex was incorporated into its physiologically relevant cargo (*Ce*IFT70/52/46/88), the motor's speed further increased to ∼1.7 µm/s in vitro (Fig. 1*B*, *iii*) (25). This full activation in fact best recapitulates the in vivo velocities of the *Ce*OSM-3 motor in the absence of the heterotrimeric kinesin-II that shares the work-load with the homodimeric *Ce*OSM-3 in the middle segment of axonemes in *C. elegans* (Fig. 1*A*) (31).

To delineate the mechanism of full activation of the autoinhibited *Ce*OSM-3 kinesin-2, we first removed its stalk and tail domains and asked whether the motor domains alone move as fast as the physiological *Ce*OSM-3-cargo complex (Fig. 1*B*, *iii*) (25). To create a double-headed motor without any potential inhibitory stalk and/or tail domains, we forced dimerization of the enzymatic motor domains (*Ce*OSM-3$^{1\text{-}349}$) with the so-called leucine zipper GCN4 (Fig. 2*A*, *Right*) (see *SI Appendix* for the protein sequences of all constructs used in this study) (32). We have additionally introduced a C-terminal GFP-tag to follow the movement of the truncated motor on surface-attached microtubules in a Total Internal Reflection Fluorescence (TIRF) microscope (Fig. 2*A*, *Right*). Indeed, the artificially dimerized motor reproduced previously observed full speed of the physiological *Ce*OSM-3-cargo complex (Fig. 2*A*, *Middle* vs. *Right* and *SI Appendix*, Movie S1) (25).

Next, we created truncations of the C-terminal stalk and tail domains to delineate the domains that are required for the inhibition of the catalytic motor domains. To this end, we monitored the respective activities of the full-length *Ce*OSM-3 and the truncated, fully active *Ce*OSM-3$^{1\text{-}349}$ motor in microtubule-activated ATPase assays. The full-length *Ce*OSM-3 remained inactive (Fig. 2*B*, dark blue diamonds), as seen previously (15). Removal of the entire stalk and tail domains significantly increased the activity of the *Ce*OSM-3$^{1\text{-}349}$ motor (Fig. 2*B*, dark blue diamonds vs. light blue circles).

To demarcate the domains responsible for the autoinhibition of the full-length *Ce*OSM-3, we next asked if the addition of the respective stalk and tail domains in trans would suffice to suppress the activity of the truncated *Ce*OSM-3$^{1\text{-}349}$ motor. The presence of the stalk domains (*Ce*OSM-3$^{350\text{-}444}$ and *Ce*OSM-3$^{445\text{-}552}$) did not alter the activity of the *Ce*OSM-3$^{1\text{-}349}$ motor (Fig. 2*B*, red vs. light blue circles). The tail domain (*Ce*OSM-3$^{553\text{-}699}$), in contrast, was sufficient to suppress the activity of the truncated *Ce*OSM-3$^{1\text{-}349}$ motor in trans (Fig. 2*B*, light blue vs. green circles).

To demonstrate the direct interaction between the motor and the tail domains, we conducted a series of microscale thermophoresis (MST) assays (33). While we observed no binding between the motor and the stalk domains (Fig. 2*C*, blue and red circles), the distal tail domain clearly displayed binding to the truncated *Ce*OSM-3$^{1\text{-}349}$ motor (Fig. 2*C*, green circles). We note however that a lack of binding in trans does not fully

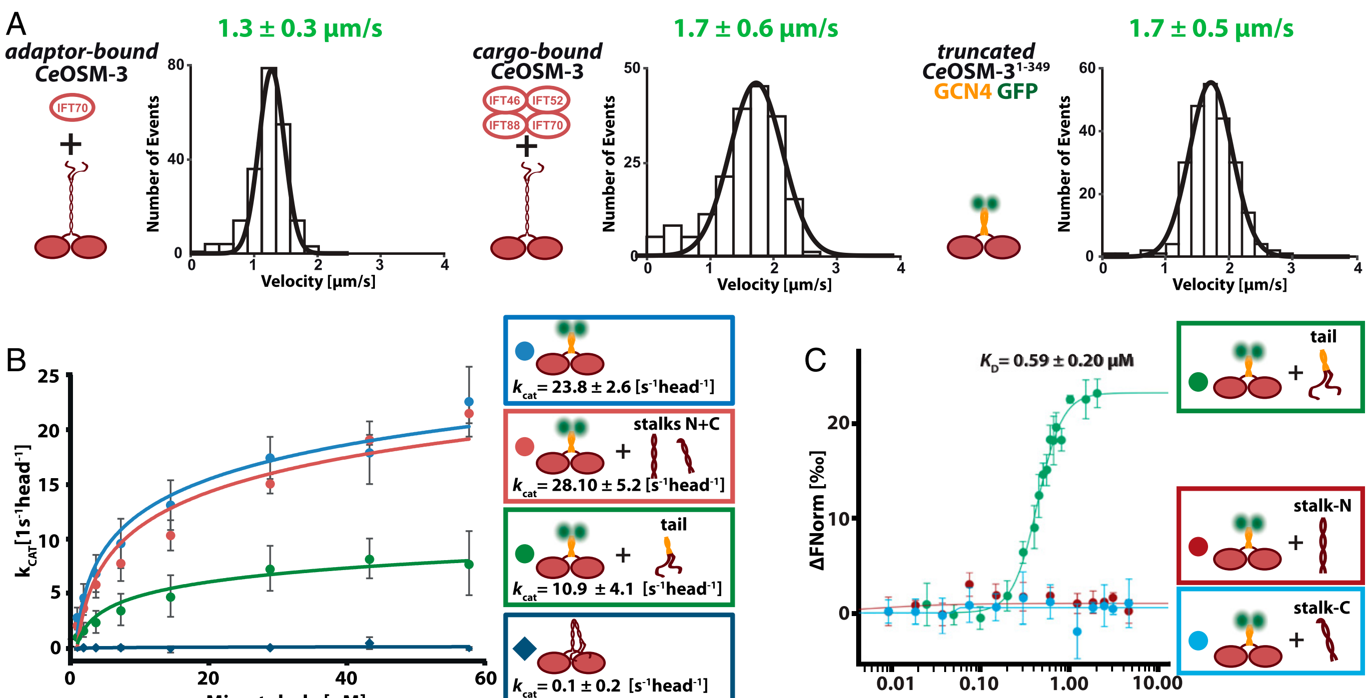

Fig. 2. The C-terminal tail domain is required for the autoinhibition of the *Ce*OSM-3 kinesin-2. (*A*) The binding of the IFT subunit *Ce*IFT70 activates the full-length motor with a velocity of 1.3 ± 0.3 µm/s (*n* = 210). *Ce*IFT70/52/46/88 fully activates the full-length motor [v = 1.7 ± 0.6 µm/s, *n* = 187, both replotted from ref. (25) for direct comparison]. Removal of the entire stalk and tail domains also fully activates the truncated *Ce*OSM-3$^{1\text{-}349}$ motor that is dimerized with an artificial coiled-coil from GCN4 (v = 1.7 ± 0.5 µm/s, *n* = 237) (see *SI Appendix*, Table S2 for all run length values that correspond to the respective velocity plots). (*B*) The full-length *Ce*OSM-3 motor does not display any significant activity in microtubule-activated ATPase assay (dark blue diamond), while the truncated, GCN4-dimerized *Ce*OSM-3$^{1\text{-}349}$ is active (light blue circle). The presence of the GCN4-dimerized tail domain (*Ce*OSM-3$^{553\text{-}699}$, green circle), but not the stalk domains (*Ce*OSM-3$^{350\text{-}444}$ and *Ce*OSM-3$^{445\text{-}552}$, red circle) inhibits the activity of the truncated *Ce*OSM-3$^{1\text{-}349}$ motor. (*C*) The fluorophore-labeled *Ce*OSM-3$^{1\text{-}349}$ motor was titrated with the tail domain *Ce*OSM-3$^{553\text{-}699}$ (green), and the respective *Ce*OSM-3$^{350\text{-}444}$ (red) and *Ce*OSM-3$^{445\text{-}552}$ stalk domains (blue) in MST assays. While the stalk domains failed to bind to the motor altogether (blue and red), the distal tail domain displayed clear binding to the truncated *Ce*OSM-3$^{1\text{-}349}$ motor (green). The velocity data points in *A* were fitted to a Gaussian distribution (± width of distribution). The data points in *C* were fitted using Hill fitting. Error bars in the ATPase and MST assays represent SD; all data obtained from three independent protein purifications each.

exclude the possibility of interaction between the head and stalk domains as the binding strength may be too weak to observe in the MST assays. Previous work in fact supports a direct interaction between the head and stalk domains in other kinesin motors, including the mammalian *Mm*KIF17 kinesin-2 ortholog of the *Ce*OSM-3 motor (14, 28).

We conclude that the motor domain alone is capable to walk as fast as the fully activated *Ce*OSM-3. The *Ce*IFT70 adaptor protein in conjunction with other cargo proteins relieves the autoinhibition of the full-length *Ce*OSM-3 motor imposed at least by the C-terminal tail domain by sequestering it via a direct interaction. We next turned to the *Ce*IFT70 adaptor protein to delineate its role in the full activation of the *Ce*OSM-3 kinesin-2 from *C. elegans*.

The *Ce*IFT70 Requires the Presence of Another Coadaptor to Fully Activate the *Ce*OSM-3 Kinesin-2. As detailed above, the full activation of the autoinhibited *Ce*OSM-3 kinesin-2 is observed only in the context of the physiological cargo complex that is formed by four different subunits (*Ce*IFT70/52/88/46) (Fig. 2*A*, *Left* vs. *Middle*) (25). Since the *Ce*IFT70 adaptor protein alone does not fully activate its motor, it is conceivable that the *Ce*IFT70 adaptor needs to interact with at least one additional subunit of the cargo complex to fully activate the *Ce*OSM-3 motor. Consistent with this notion, the *Ce*IFT70 ortholog from *C. reinhardtii* (*Cr*IFT70) was shown to wrap around a short, proline-rich stretch of the conserved *Cr*IFT52 protein in a previous high-resolution crystal structure (34). We therefore asked whether this rather unusual interaction between the *Cr*IFT70 and the *Cr*IFT52 proteins plays any direct role in the full activation of the *Ce*OSM-3 motor. To test this possibility, we labeled the respective *C. elegans* orthologs (*Ce*IFT70 and *Ce*IFT52) with different fluorophores, along with the *Ce*IFT88 subunit of the physiological cargo complex as a control (Fig. 3 *A* and *B*, *Left*). Dual tracking of the differentially labeled adaptor subunits ensured that the data are obtained exclusively from the motors each bound to both, *Ce*IFT70/52 or *Ce*IFT70/88 complexes, respectively.

In the absence of any adaptor protein, *Ce*OSM-3 remained autoinhibited and was incapable of directional movement (*SI Appendix*, Movie S2, *Top Left*) as expected from previous work (15, 25). The presence of the respective adaptor complexes *Ce*IFT70/52 and *Ce*IFT70/88 activated the *Ce*OSM-3 motor (*SI Appendix*, Movie S2, *Top Right* and *Bottom Left*).

However, presence of the *Ce*IFT88 subunit, in addition to *Ce*IFT70, failed to fully activate the *Ce*OSM-3, and the motor moved at a comparatively slow speed of ∼1.2 μm/s (Fig. 3*A*), which is similar to what has been observed by the *Ce*IFT70-mediated activation (Fig. 3*A* vs. 2*A*, *Left*) (25). In contrast, the presence of the *Ce*IFT52 subunit, in addition to *Ce*IFT70, was necessary and sufficient to reproduce the previously observed full activation of the autoinhibited *Ce*OSM-3 by its physiological complex (Fig. 3*B* vs. 2*A*, *Middle*) (25). Consistent with the C-terminal random coil being involved in the autoinhibition of the *Ce*OSM-3 motor (Fig. 2 *B* and *C*), the *Ce*IFT70/52 adaptor complex coprecipitated with the random coil domain and not with the coiled-coil stalks or the motor domains (*SI Appendix*, Fig. S3).

We next tested if *Ce*IFT70/52 could stimulate a mutated version of the motor, *Ce*OSM-3^{G444E} (Fig. 1*B*, i). This mutation is known to activate the motor by preventing autoinhibitory folding and allows it to walk with ∼1.1 to 1.2 μm/s (15, 25). Binding of *Ce*IFT70 alone did not suffice to stimulate the velocity of *Ce*OSM-3^{G444E}, however, *Ce*IFT70/52 stimulated

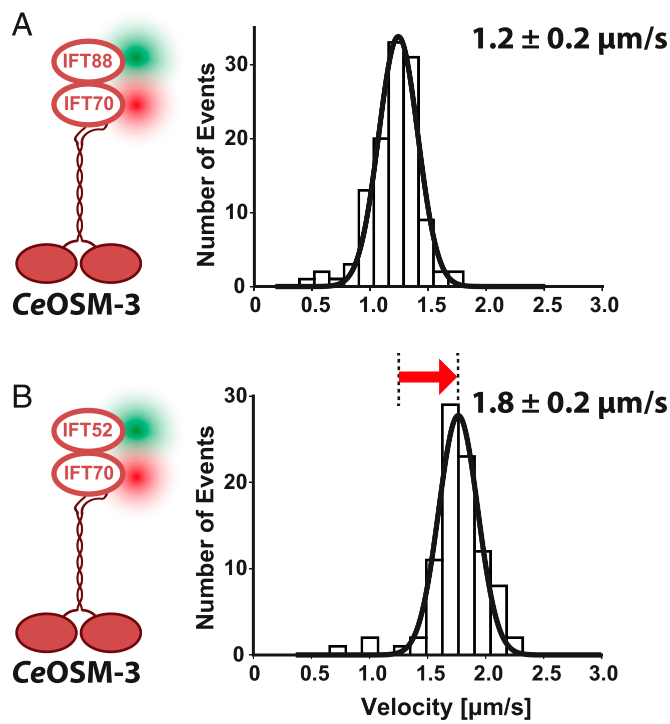

Fig. 3. *Ce*IFT70 and *Ce*IFT52 subunits are necessary and sufficient for the full activation of the *Ce*OSM-3 motor. (*A* vs. *B*) *Ce*IFT70^{SNAP647} fully activates the *Ce*OSM-3 motor only in the presence of *Ce*IFT52^{GFP} (*B*, v = 1.8 ± 0.2 μm/s, *n* = 91) but not in the presence of the *Ce*IFT88^{GFP} subunit of the physiological cargo complex (*A*, v = 1.2 ± 0.2 μm/s, N = 117). Velocity data were fitted to a Gaussian (± width of distribution) distribution (see *SI Appendix*, Table S3*A* for two-sample *t* tests of the velocities). Data were obtained from three independent protein preparations each.

also this version of the motor to move with 1.7 ± 0.3 μm/s as expected (*SI Appendix*, Fig. S4 *A* vs. *B*). In contrast, neither *Ce*IFT70/88 nor *Ce*IFT70/46 could further stimulate the partially activated *Ce*OSM-3^{G444E} (*SI Appendix*, Fig. S4 *C* and *D*), underscoring the significance of the complex formation between the *Ce*IFT70 and the *Ce*IFT52 subunits in the full activation of the *Ce*OSM-3 motor.

Importantly, the activating potentials of *Ce*IFT70/52 and the G444E mutation were not additive to each other because velocities did not exceed 1.7 μm/s for the *Ce*IFT70/52-bound *Ce*OSM-3^{G444E} motor. We therefore suggest that both *Ce*IFT70/52 and the G444E mutation influence steps in the same pathway toward relieve of autoinhibition. Lack of additivity also rules out a simple model in which the motor exists in only two states, fully inhibited or fully active, and in which intermediate velocities manifest themselves by a rapid switch between these states. Instead, at least three states must exist to explain the data, a fully inhibited state, a structural intermediate and a fully active state (*SI Appendix*, Fig. S4*E*). In the simplest version of this three-state model, the structural intermediate moves at intermediate velocities of ∼1.2 μm/s, but scenarios in which it walks with much lower velocity are theoretically possible. The three-state model also implies that *Ce*OSM-3 is autoinhibited by at least two different mechanisms. Above, we provide evidence for tail-domain mediated autoinhibition of the motor (Fig. 2). The nature of the second autoinhibitory mechanism remains to be explored in more detail in future studies.

Molecular Determinants of Allosteric Activation by the IFT70/52 Cargo Adaptor. To better understand the specific role of the IFT70/52 adaptor complex, we next created mutants to delineate the regions in the respective subunits that are required for the allosteric activation of the *Ce*OSM-3 motor. To this end, we turned to the high-resolution crystal structure of the orthologous IFT70/52 adaptor complex from *C. reinhardtii* where *Cr*IFT70 was shown to wrap around a short and conserved proline-rich stretch in the *Cr*IFT52 subunit (34). Notably, removal of this corresponding region in the *Ce*IFT52 subunit (*Ce*IFT52$^{\Delta 322\text{-}376}$) abolished the full activation of the *Ce*OSM-3 motor, while the short peptide containing the conserved proline-rich region alone (*Ce*IFT52$^{322\text{-}380}$) was sufficient for full activation (*SI Appendix*, Figs. S5*A* and S6). These results underscore the functional relevance of the evolutionary conserved proline-rich region and suggests that the peculiar way how the *Cr*IFT70 subunit wraps around this stretch in the *Cr*IFT52 protein from the *C. reinhardtii* model (34) might also take place in the respective orthologs from *C. elegans*.

Intrigued by this functional interdependence between the *Ce*IFT70 and *Ce*IFT52 subunits of the physiological cargo complex (Fig. 1*B*, *iii*), we next turned to the *Ce*IFT70 adaptor protein to unmask the determinants that contribute to the full activation of the autoinhibited *Ce*OSM-3 motor in the presence of the *Ce*IFT52 subunit (Fig. 3). To this end, we focused on a particularly conspicuous repetitive tyrosine motif in the N terminus of the *Ce*IFT70 adaptor protein that is conserved between distantly related eukaryotes (*SI Appendix*, Fig. S7) (34, 35). The aromatic rings of these repetitive tyrosines were found to tightly stack against the highly conserved proline-rings in the aforementioned proline-rich stretch of the *Cr*IFT52 subunit as seen in the high-resolution structure from the *C. reinhardtii* model (Fig. 4*A*) (34). Because this stacking was proposed to stabilize the predominantly hydrophobic interface between the *Cr*IFT70 and *Cr*IFT52 orthologs from *C. reinhardtii* (34), we asked whether interfering with this conserved interface in the *Ce*IFT70 and *Ce*IFT52 orthologs from *C. elegans* has any functional consequences for the full activation of the *Ce*OSM-3 motor.

To test this hypothesis, we mutated four tyrosines into alanines in the *Ce*IFT70 subunit (Fig. 4*B*). The alanine mutations in the *Ce*IFT70 adaptor abolished the *Ce*IFT70/52 mediated full activation, and the *Ce*OSM-3 moved at decreased speeds that were consistent with the *Ce*IFT70-mediated activation of the motor (Fig. 4 *D* vs. *C* and *SI Appendix*, Fig. S5*B* and Movie S3, *Left*) (25). We rescued the full activation of *Ce*OSM-3, however, by mutating the tyrosines into phenylalanines instead of alanines (Fig. 4 *E* vs. *D* and *SI Appendix*, Fig. S5*B* and Movie S3, *Right*). Phenylalanine is in fact structurally similar to tyrosine, except that it lacks the hydroxyl group on the aromatic ring. Based on the capability of phenylalanines to fully substitute the function of wild type tyrosines, we propose that the hydrophobic stacking between the tyrosines in *Ce*IFT70 and prolines in *Ce*IFT52, as seen in the *C. reinhardtii* proteins (34), is necessary and sufficient for the full activation of the *Ce*OSM-3 motor. Consistently, the N-terminally truncated *Ce*IFT70b$^{\Delta 1\text{-}59}$ that lacks the conserved tyrosine motif failed to fully activate *Ce*OSM-3 (*SI Appendix*, Table S1*B* and Figs. S8 and S5*C*).

Yet, the presence of such potentially functional interaction between the *Cr*IFT70 and *Cr*IFT52 subunits from the green algae *C. reinhardtii* is puzzling given that it solely deploys a heterotrimeric kinesin-2 motor that in turn is recruited to the IFT trains via the Kinesin Associated Protein (KAP) (*SI Appendix*, Fig. S1, *Top*) (6–8). In contrast, a homodimeric kinesin-2 is deployed in the mouse model. However, the mouse motor appears to be inactive inside the cilium despite the presence of the IFT70/52 adaptor complex (*SI Appendix*, Fig. S1, *Bottom*).

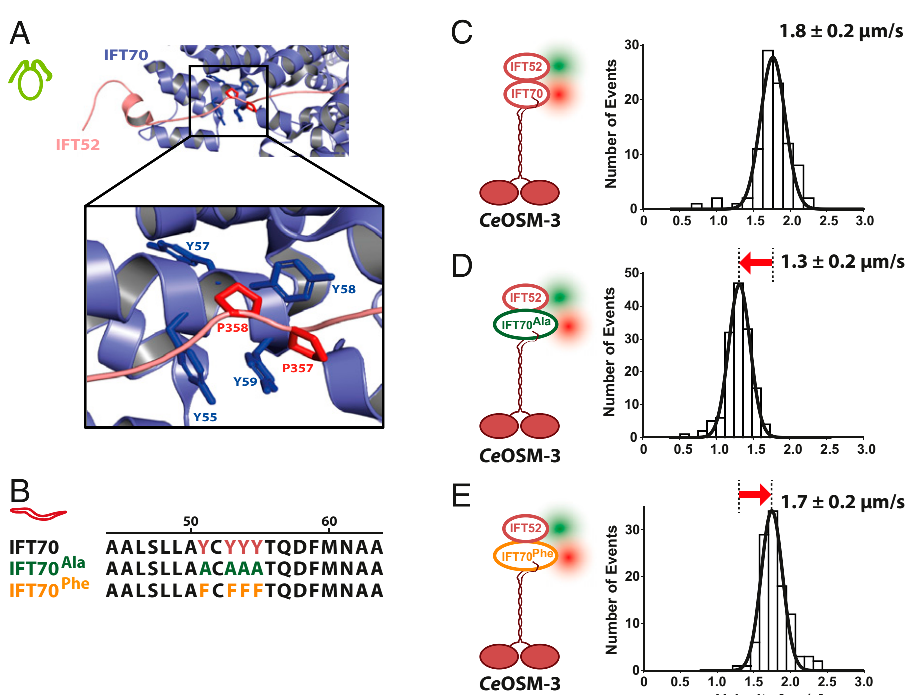

Fig. 4. The evolutionary conserved tyrosines in *Ce*IFT70 are key to the full activation of the *Ce*OSM-3 kinesin-2. (*A*) A conserved tyrosine motif Y55,57,58,59 of *Cr*IFT70 forms an exceptional stacking arrangement with the proline rings of P357,358 in *Cr*IFT52 in the high-resolution crystal structure from Taschner et al. (34). (*B*) Sequence alignment of the repetitive tyrosines (see also *SI Appendix*, Fig. S7) in the wild-type *Ce*IFT70 (top lane) with the *Ce*IFT70^{Ala} mutant Y51/53/54/55A (green) and *Ce*IFT70^{Phe} mutant Y51/53/54/55F (orange), respectively. (*C*) The full activation of the *Ce*OSM-3 motor by the wild-type *Ce*IFT70/52 adaptor complex replotted from Fig. 3*B* for direct comparison. (*D*) Mutating the wild-type tyrosines into alanines in *Ce*IFT70^{Ala,SNAP647} prevents the full activation of the *Ce*OSM-3 motor (v = 1.3 ± 0.2 µm/s, *n* = 145). (*E*) The full activation of *Ce*OSM-3 is rescued by replacing the alanines with phenylalanines in *Ce*IFT70^{Phe,SNAP647} (v = 1.7 ± 0.2 µm/s, *n* = 109). Velocity data were fitted to a Gaussian (± width of distribution) distribution (see *SI Appendix*, Table S3A for the corresponding two-sample *t* tests). Data were obtained from three independent protein preparations each.

We next turned to the *C. reinhardtii* and mouse models to assess the functional relationship between the kinesin-2 orthologs and the IFT70/52 cargo adaptor, respectively.

The Adaptor Function, and not the Kinesin-2 Motor, is Kept Conserved. To our surprise, not only did the respective *Cr*IFT70/52 and *Mm*IFT70/52 adaptor complexes from *C. reinhardtii* and mouse activate the *Ce*OSM-3 motor from *C. elegans*, but the activation levels were indistinguishable from the worm *Ce*IFT70/52 adaptor complex (Fig. 5 and *SI Appendix*, Figs. S5 *D* and *E*, S9, and S10 and Movie S4). This remarkable functional equivalency suggests that a functional on-switch for the homodimeric kinesin-2 motor from the multicellular *C. elegans* may have developed early and kept conserved throughout the evolution. Given that the adaptor complex from mouse was fully functional, we next dissected the behavior of the mouse kinesin-2 to assess whether the same activation adaptor-mediated activation mechanism also applies to this particular motor.

As seen previously with the respective kinesin-2 motors from *C. elegans* and mouse (*SI Appendix*, Movies S2, *Top Left* and S5, *Left*) (14, 15), the *Mm*KIF17 kinesin-2 did not display any directional movement. It only diffused along the surface-attached microtubules (*SI Appendix*, Movie S5, *Left*). This behavior is consistent with the full-length *Mm*KIF17 motor being autoinhibited (14). If true, disengagement of the inhibitory C terminus either by binding to an artificial cargo or simply by its C-terminal truncation should activate the *Mm*KIF17 motor. Indeed, surface attachment of the full-length *Mm*KIF17 via its C terminus as well as the C-terminal truncation *Mm*KIF17$^{1\text{-}747}$ activated the respective motors to levels that were consistent with previous in vivo studies (*SI Appendix*, Movies S5, *Right*, S6, and Fig. S11 *A* and *B*) (14, 36, 37). These results demonstrate that the recombinantly expressed *Mm*KIF17 construct is functional in our reconstitution assays and suggests that the diffusive behavior of the full-length motor results from the C terminus-mediated autoinhibition, consistent with previous results (14).

Next, we asked whether the autoinhibited *Mm*KIF17 interacts with *Mm*IFT70, and if so, whether this interaction relieves the autoinhibition of the motor to allow directional transport. To this end, we first assessed if *Mm*KIF17 motors colocalize efficiently with the *Mm*IFT70 adaptor protein (*SI Appendix*, Table S1*B*). In particular, we tested the full-length *Mm*KIF17 along with the truncated *Mm*KIF17$^{1\text{-}747}$ motor that lacked its C terminus as a control for C-terminal adaptor binding (*SI Appendix*, Fig. S11*C*). *Mm*KIF17 with or without its C terminus did not efficiently colocalize with the *Mm*IFT70 protein and its serial orthologs *Mm*IFT70A2 and *Mm*IFT70B (*SI Appendix*, Table S1*B*), suggesting that the motor-adaptor protein pair has lost their ability to interact with each other in the course of evolution (*SI Appendix*, Fig. S11*C*, lanes I to IV), nor did *Mm*KIF17 interact with the *Ce*IFT70 (*SI Appendix*, Fig. S11*C*, lane V). In functional transport assays, the *Mm*KIF17 motor failed to display any colocalized movement with the *Mm*IFT70 adaptor and consequently remained autoinhibited (*SI Appendix*, Movie S7, *Left*). In stark contrast, the *Ce*OSM-3 motor displayed a significant colocalization with the distantly related mouse *Mm*IFT70 adaptor (*SI Appendix*, Fig. S11*C*, lane VI) as expected from the ability of the mouse adaptor to activate the *Ce*OSM-3 motor from *C. elegans* (Fig. 5 and *SI Appendix*, Figs. S9 *C* and *D* and S10).

Based on our findings from functional reconstitution assays, we therefore propose that loss of activation of the mouse kinesin-2 motor by its adaptor arose from the diversification of the kinesin-2 motor and not the cargo adaptor. Specifically, *Mm*KIF17 motor evolved to lose its ability to interact with the *Mm*IFT70 adaptor for activation, and consequently behaves as an inactive passenger of the IFT trains in the mammalian cilium (*SI Appendix*, Fig. S1, *Bottom*). However, at this point, it cannot be fully excluded that *Mm*KIF17 employs other activation mechanisms during IFT in a cell type-specific manner.

Intrigued by the striking conservation of the IFT70/52 adaptor function (Fig. 5), we turned to the KAP that is known to function as a universal adaptor for the heterotrimeric kinesin-2 motors (3, 38). In particular, we asked if the functional compatibility that we observed between the homodimeric kinesin-2 and the IFT70/52 adaptor extends to this paralogous class of kinesin-2 motors as well. To this end, we tested if the heterodimeric *Ce*KLP11/20, which powers IFT together with the homodimeric kinesin-2 in *C. elegans* (*SI Appendix*, Fig. S1, *Middle*), retains the ability to interact with the orthologous KAP proteins from *C. reinhardtii* and mouse, respectively. Whereas *Ce*KAP bound *Ce*KLP11/20 as expected from previous in vivo and in vitro work (9, 39, 40), the KAP adaptors from *C. reinhardtii* and mouse did not (*SI Appendix*, Fig. S12*A*).

Functionally, KAP binding to the heterodimeric kinesin-2 motors also leads to varying effects. *Ce*KAP did not kinetically activate the *Ce*KLP11/20 motor in single molecule assays (*SI Appendix*, Fig. S12*B*), in line with results obtained for the

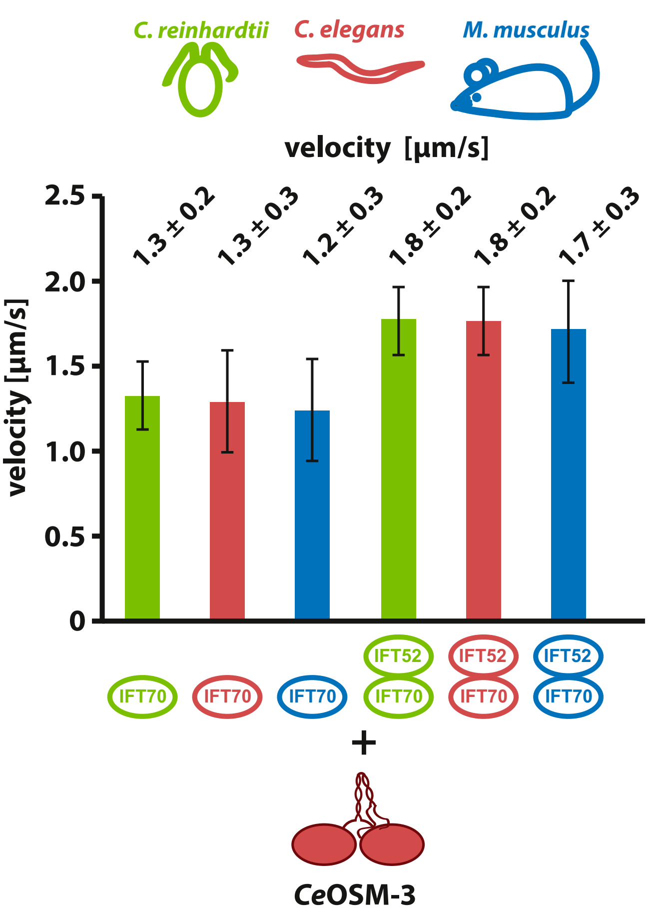

Fig. 5. *C. reinhardtii* and mouse adaptors phenocopy the function of the *C. elegans* adaptors *Ce*IFT70 and *Ce*IFT70/52 in vitro. The autoinhibited *Ce*OSM-3 motor is activated by the IFT70 and IFT70/52 adaptors from the distantly related *C. reinhardtii* and mouse (see *SI Appendix*, Fig. S9 for the respective velocity distributions and values). The respective *Cr*IFT70 and *Mm*IFT70 adaptors along with the *Cr*IFT70/52 and *Mm*IFT70/52 adaptor complexes reproduce the behavior of the worm *Ce*IFT70 and *Ce*IFT70/52 proteins in functional reconstitution assays (see *SI Appendix*, Fig. S10 for the functional equivalency of the serial orthologs of *Mm*IFT70).

corresponding mouse ortholog, heterodimeric *Mm*KIF3A/3B kinesin-2 (41). In contrast, the KAP adaptor from *C. reinhardtii* fully activated the heterodimeric *Cr*FLA8/10 motor as we demonstrated recently in functional reconstitution studies (8).

In summary, we discovered that IFT70/52-adaptor binding and the ensuing activation of homodimeric kinesin-2 motors is much more conserved than KAP-adaptor binding and its effects on heterodimeric kinesin-2 motors. These findings demonstrate that the recruitment and activation mechanism of kinesin-2 motors are complex and must be clarified experimentally in a case-to-case basis.

A Functional Cargo-Motor Interface has been Established Early in the Evolution. *C. elegans* is so far the only model organism where the use of a homodimeric kinesin-2 during the IFT process has been demonstrated conclusively (*SI Appendix*, Fig. S1) (3, 9, 40). Given the presence of a functional cargo adaptor already in the green algae *C. reinhardtii*, we considered the possibility that IFT70/52-regulated kinesin-2 transport predates metazoan evolution. In fact, phylogenetic analyses predict the existence of a number of kinesin-2 motors in several unicellular organisms (3, 42). Yet, whether the predicted proteins assemble into heterotrimeric or homodimeric kinesin-2 motors cannot be determined by sequence analysis, and instead requires recombinant reconstitution or tissue purification (38, 39, 43–45). The unicellular ciliate *Tetrahymena thermophila* represents a particularly interesting case as it harbors an unusually high number of six kinesin-2 motors in its genome (3, 42). While three kinesin-2 motors (i.e., Kin5, KIN1, and KIN2) have been implicated in IFT in previous in vivo studies (46–48), the oligomerization and regulation mechanism of kinesin-2 motors in *T. thermophila* remain unknown. The *Tt*Kin5, in particular, was suggested to be orthologous to the *Ce*OSM-3, and consistent with its proposed function as a ciliary kinesin-2, *Tt*Kin5 was up-regulated after deciliation and localized along the ciliary axoneme (46). Of note, the orthologous IFT70 adaptor from this organism also contains the conserved tyrosine motif that is essential for the allosteric activation of the *Ce*OSM-3 motor (*SI Appendix*, Fig. S7), suggesting that it may function as a cargo adaptor for the *Tt*Kin5 motor. Further supporting this notion, *T. thermophila* only assembled short axonemes in the absence of *ift70* function (49), resembling the phenotype seen in *C. elegans* where the absence of *ift70* also leads to short cilia (24). We therefore turned to our reconstitution assays to directly contrast the activation mechanisms of kinesin-2 orthologs between the distantly related *T. thermophila* and *C. elegans* models.

Recombinantly expressed full-length *Tt*Kin5 was homodimeric as judged from size-exclusion chromatography coupled to multiple-angle light scattering (SEC-MALS) analysis (*SI Appendix*, Fig. S13*A*), and moved microtubules in gliding filament assays with a velocity of ∼2 μm/s (*SI Appendix*, Fig. S13*B* and Movie S8). Consistent with *Tt*Kin5 forming a functional homodimeric kinesin-2, it displayed processive motility on surface-attached microtubules (*SI Appendix*, Movie S9, *Top Left*). In contrast to *Ce*OSM-3, however, it does not rely on other proteins to become active. Nevertheless, the *Tt*Kin5 motor moved substantially slower on surface attached microtubules (∼1.4 μm/s; *SI Appendix*, Fig. S13*C*) when compared to its microtubule gliding velocity (∼2 μm/s, *SI Appendix*, Fig. S13*B*), hinting at potential autoinhibition that was relieved by surface attachment in the filament gliding assay as illustrated in *SI Appendix*, Fig. S13*B*, *Left*.

If the surface attachment represents the full activation of *Tt*Kin5, and if the *Tt*IFT70/52 functions as a cargo adaptor of this kinesin-2 from *T. thermophila*, then a trimeric complex of *Tt*Kin5 with *Tt*IFT70/52 would be expected to form and move at a velocity of ∼2 μm/s. This is what we could observe in the presence of *Tt*IFT70/52, but not the *Tt*IFT70 subunit alone (Fig. 6 *A* vs. *B* and *SI Appendix*, Fig. S5*F* and Movie S9, *Top Right* vs. *Bottom Left*). We note the remarkable functional equivalency between

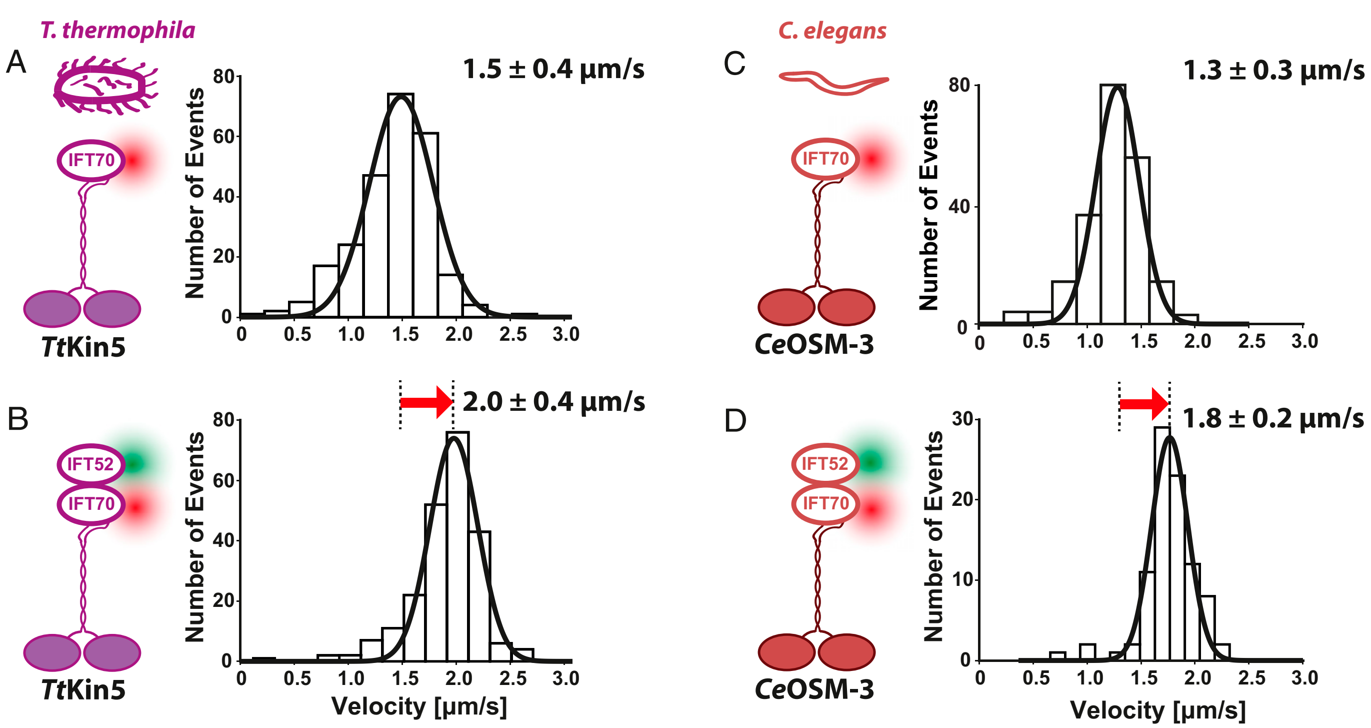

Fig. 6. The ciliate *T. thermophila* and the metazoan *C. elegans* share a common mechanism of allosteric motor activation. (*A* vs. *B*) The presence of the *Tt*IFT70 and *Tt*IFT52 subunits is necessary and sufficient to fully activate the homodimeric *Tt*Kin5 kinesin-2 from *T. thermophila* (*A*, v = 1.5 ± 0.4 μm/s, *n* = 250; *B*, v = 2.0 ± 0.3 μm/s, *n* = 226), just like the *Ce*OSM-3 kinesin-2 from *C. elegans* (*C* vs. *D*, replotted from Figs. 2*A* and 3*B* to facilitate direct comparison to the *T. thermophila* model). Velocity data were fitted to a Gaussian (± width of distribution) distribution (see *SI Appendix*, Table S3C for two-sample *t* tests of the velocities). Data were obtained from three independent protein preparations each.

the *Ce*IFT70/52-mediated activation of the *Ce*OSM-3 and the *Tt*IFT70/52-mediated activation of the *Tt*Kin5 kinesin-2 motors (Fig. 6 *A*/*B* vs. *C*/*D*). Even the magnitude of the stimulatory effect is similar.

Together with previous in vivo work (46), results from our reconstitution studies make a strong case that the ciliate *T. thermophila* model deploys at least one homodimeric kinesin-2 during IFT. However, *T. thermophila* uses two more kinesin-2 motors (KIN1 and KIN2) for the IFT process that seem to work redundantly, i.e., only the knockout of both motors leads to almost complete loss of cilia in vivo (48). Given that *T. thermophila* is predicted to have at least three more kinesin-2 motors (3), it is likely that the ciliary deployment of the heterotrimeric and/or homodimeric kinesin-2 motors is redundant in this unicellular eukaryote, conceptually similar to what has been observed in the *C. elegans* (3, 9).

The fact that kinesin-2 motors from a ciliate (*Tt*Kin5) and from a multicellular animal (*Ce*OSM-3) share the same activation mechanism suggests that homodimeric kinesin-2 deployment and IFT70/52-mediated regulation has been an early evolutionary invention to power IFT. Mouse *Mm*KIF17 kinesin-2 represents a remarkable outlier to this strictly conserved machinery, despite being a close ortholog of *Ce*OSM-3 (42). In other words, relatively recent changes occurred in the mouse *Mm*KIF17 kinesin-2 that disrupted the canonical interface between the motor and its adaptor (*SI Appendix*, Fig. S11*C* and Movie S7, *Left*). Evolutionary relatedness of the kinesin-2 motor domains therefore cannot fully predict their activation mechanisms, and as concluded above, must be determined experimentally on a case-to-case basis (*SI Appendix*, Fig. S14).

Taken together, our results warrant a closer look at the homodimeric kinesin-2 that is considered as an accessory motor of the IFT process in multicellular animals. It will be important to explore further whether the common allosteric activation mechanism of the kinesin-2 motor, which we show is shared between the ciliate *T. thermophila* and the multicellular animal *C. elegans*, also applies to other organisms. We predict that the role of the homodimeric kinesin-2 motor may be underappreciated and that it plays a more fundamental role in the IFT process than previously recognized.

Data Materials, and Software Availability. Microscopy movies that are used for the analyses are included in the supplementary data. The corresponding original movie files are available from the corresponding author upon request. Datasets generated during and/or analyzed during the current study, along with all study-specific reagents are available from the corresponding author upon request. All other study data are included in the article and/or supporting information.

ACKNOWLEDGMENTS. We thank Günther Woehlke (Technische Universität München) for fruitful discussions on kinesin-2 motors. We also thank Thi-Hieu Ho, Punam Sonar, and Mohamed Antar Aziz Mohamed (Technische Universität München) for their help in virus generation. This work was supported by the European Research Council grant 335623 and by Deutsche Forschungsgemeinschaft (DFG) grant SFB863, project ID 111166240 to Z.Ö. and DFG grant MU3613/1-2 to F.M.-P.

Author affiliations: [a]Center for Protein Assemblies (CPA), Physics Department, E22, Technical University of Munich, Garching, 85748, Germany; and [b]Institute of Physiological Chemistry, Faculty of Medicine Carl Gustav Carus, Technische Universität Dresden, Dresden, 01307, Germany

1. D. R. Mitchell, The evolution of eukaryotic cilia and flagella as motile and sensory organelles. *Adv. Exp. Med. Biol.* **607**, 130–140 (2007).
2. M. Taschner, E. Lorentzen, The intraflagellar transport machinery. *Cold Spring Harb. Perspect. Biol.* **8**, a028092 (2016).
3. J. M. Scholey, Kinesin-2: A family of heterotrimeric and homodimeric motors with diverse intracellular transport functions. *Annu. Rev. Cell Dev. Biol.* **29**, 443–469 (2013).
4. S. Webb, A. G. Mukhopadhyay, A. J. Roberts, Intraflagellar transport trains and motors: Insights from structure. *Semin. Cell Dev. Biol.* **107**, 82–90 (2020).
5. Z. Walther, M. Vashishtha, J. L. Hall, The Chlamydomonas FLA10 gene encodes a novel kinesin-homologous protein. *J. Cell Biol.* **126**, 175–188 (1994).
6. K. G. Kozminski, P. L. Beech, J. L. Rosenbaum, The Chlamydomonas kinesin-like protein FLA10 is involved in motility associated with the flagellar membrane. *J. Cell Biol.* **131**, 1517–1527 (1995).
7. J. Mueller, C. A. Perrone, R. Bower, D. G. Cole, M. E. Porter, The FLA3 KAP subunit is required for localization of kinesin-2 to the site of flagellar assembly and processive anterograde intraflagellar transport. *Mol. Biol. Cell* **16**, 1341–1354 (2005).
8. P. Sonar *et al.*, Kinesin-2 from *C. reinhardtii* is an atypically fast and auto-inhibited motor that is activated by heterotrimerization for intraflagellar transport. *Curr. Biol.* **30**, 1160–1166.e5 (2020).
9. D. Signor, K. P. Wedaman, L. S. Rose, J. M. Scholey, Two heteromeric kinesin complexes in chemosensory neurons and sensory cilia of *Caenorhabditis elegans*. *Mol. Biol. Cell* **10**, 345–360 (1999).
10. M. F. Engelke *et al.*, Acute inhibition of heterotrimeric kinesin-2 function reveals mechanisms of intraflagellar transport in mammalian cilia. *Curr. Biol.* **29**, 1137–1148.e4 (2019).
11. T. Funabashi *et al.*, Ciliary entry of KIF17 is dependent on its binding to the IFT-B complex via IFT46-IFT56 as well as on its nuclear localization signal. *Mol. Biol. Cell* **28**, 624–633 (2017).
12. L. Jiang *et al.*, Kinesin family 17 (osmotic avoidance abnormal-3) is dispensable for photoreceptor morphology and function. *FASEB J.* **29**, 4866–4880 (2015).
13. C. L. Williams *et al.*, Direct evidence for BBSome-associated intraflagellar transport reveals distinct properties of native mammalian cilia. *Nat. Commun.* **5**, 5813 (2014).
14. J. W. Hammond, T. L. Blasius, V. Soppina, D. Cai, K. J. Verhey, Autoinhibition of the kinesin-2 motor KIF17 via dual intramolecular mechanisms. *J. Cell Biol.* **189**, 1013–1025 (2010).
15. M. Imanishi, N. F. Endres, A. Gennerich, R. D. Vale, Autoinhibition regulates the motility of the C. elegans intraflagellar transport motor OSM-3. *J. Cell Biol.* **174**, 931–937 (2006).
16. R. D. Vale, The molecular motor toolbox for intracellular transport. *Cell* **112**, 467–480 (2003).
17. K. J. Verhey, J. W. Hammond, Traffic control: Regulation of kinesin motors. *Nat. Rev. Mol. Cell Biol.* **10**, 765–777 (2009).
18. D. V. Trivedi, S. Nag, A. Spudich, K. M. Ruppel, J. A. Spudich, The myosin family of mechanoenzymes: From mechanisms to therapeutic approaches. *Annu. Rev. Biochem.* **89**, 667–693 (2020).
19. S. Tafoya, C. Bustamante, Molecular switch-like regulation in motor proteins. *Philos. Trans. R. Soc. Lond. B Biol. Sci.* **373**, 20170181 (2018).
20. A. Akhmanova, J. A. Hammer, 3rd, Linking molecular motors to membrane cargo. *Curr. Opin. Cell Biol.* **22**, 479–487 (2010).
21. J. A. Cross, M. P. Dodding, Motor-cargo adaptors at the organelle-cytoskeleton interface. *Curr. Opin. Cell Biol.* **59**, 16–23 (2019).
22. M. M. Fu, E. L. Holzbaur, Integrated regulation of motor-driven organelle transport by scaffolding proteins. *Trends Cell Biol.* **24**, 564–574 (2014).
23. N. Hirokawa, Y. Noda, Y. Tanaka, S. Niwa, Kinesin superfamily motor proteins and intracellular transport. *Nat. Rev. Mol. Cell Biol.* **10**, 682–696 (2009).
24. G. Ou, O. E. Blacque, J. J. Snow, M. R. Leroux, J. M. Scholey, Functional coordination of intraflagellar transport motors. *Nature* **436**, 583–587 (2005).
25. M. A. A. Mohamed, W. L. Stepp, Z. Ökten, Reconstitution reveals motor activation for intraflagellar transport. *Nature* **557**, 387–391 (2018).
26. K. Boldt *et al.*; UK10K Rare Diseases Group, An organelle-specific protein landscape identifies novel diseases and molecular mechanisms. *Nat. Commun.* **7**, 11491 (2016).
27. H. Y. Kaan, D. D. Hackney, F. Kozielski, The structure of the kinesin-1 motor-tail complex reveals the mechanism of autoinhibition. *Science* **333**, 883–885 (2011).
28. J. Ren *et al.*, Coiled-coil 1-mediated fastening of the neck and motor domains for kinesin-3 autoinhibition. *Proc. Natl. Acad. Sci. U.S.A.* **115**, E11933–E11942 (2018).
29. M. Schliwa, G. Woehlke, Molecular motors. *Nature* **422**, 759–765 (2003).
30. S. Adio, J. Reth, F. Bathe, G. Woehlke, Review: Regulation mechanisms of Kinesin-1. *J. Muscle Res. Cell Motil.* **27**, 153–160 (2006).
31. B. Prevo, P. Mangeol, F. Oswald, J. M. Scholey, E. J. Peterman, Functional differentiation of cooperating kinesin-2 motors orchestrates cargo import and transport in *C. elegans* cilia. *Nat. Cell Biol.* **17**, 1536–1545 (2015).
32. E. K. O'Shea, J. D. Klemm, P. S. Kim, T. Alber, X-ray structure of the GCN4 leucine zipper, a two-stranded, parallel coiled coil. *Science* **254**, 539–544 (1991).
33. M. Jerabek-Willemsen *et al.*, MicroScale thermophoresis: Interaction analysis and beyond. *J. Mol. Struct.* **1077**, 101–113 (2014).
34. M. Taschner, F. Kotsis, P. Braeuer, E. W. Kuehn, E. Lorentzen, Crystal structures of IFT70/52 and IFT52/46 provide insight into intraflagellar transport B core complex assembly. *J. Cell Biol.* **207**, 269–282 (2014).
35. Z. C. Fan *et al.*, Chlamydomonas IFT70/CrDYF-1 is a core component of IFT particle complex B and is required for flagellar assembly. *Mol. Biol. Cell* **21**, 2696–2706 (2010).
36. R. W. Wong, M. Setou, J. Teng, Y. Takei, N. Hirokawa, Overexpression of motor protein KIF17 enhances spatial and working memory in transgenic mice. *Proc. Natl. Acad. Sci. U.S.A.* **99**, 14500–14505 (2002).
37. L. Guillaud, M. Setou, N. Hirokawa, KIF17 dynamics and regulation of NR2B trafficking in hippocampal neurons. *J. Neurosci.* **23**, 131–140 (2003).
38. D. G. Cole *et al.*, Novel heterotrimeric kinesin-related protein purified from sea urchin eggs. *Nature* **366**, 268–270 (1993).
39. X. Pan *et al.*, Mechanism of transport of IFT particles in *C. elegans* cilia by the concerted action of kinesin-II and OSM-3 motors. *J. Cell Biol.* **174**, 1035–1045 (2006).
40. J. J. Snow *et al.*, Two anterograde intraflagellar transport motors cooperate to build sensory cilia on *C. elegans* neurons. *Nat. Cell Biol.* **6**, 1109–1113 (2004).
41. H. Yamazaki, T. Nakata, Y. Okada, N. Hirokawa, Cloning and characterization of KAP3: A novel kinesin superfamily-associated protein of KIF3A/3B. *Proc. Natl. Acad. Sci. U.S.A.* **93**, 8443–8448 (1996).
42. B. Wickstead, K. Gull, T. A. Richards, Patterns of kinesin evolution reveal a complex ancestral eukaryote with a multifunctional cytoskeleton. *BMC Evol. Biol.* **10**, 110 (2010).
43. M. A. Berezuk, T. A. Schroer, Fractionation and characterization of kinesin II species in vertebrate brain. *Traffic* **5**, 503–513 (2004).

44. M. Brunnbauer *et al.*, Regulation of a heterodimeric kinesin-2 through an unprocessive motor domain that is turned processive by its partner. *Proc. Natl. Acad. Sci. U.S.A.* **107**, 10460–10465 (2010).
45. M. Brunnbauer *et al.*, Torque generation of kinesin motors is governed by the stability of the neck domain. *Mol. Cell* **46**, 147–158 (2012).
46. A. Awan, M. Bernstein, T. Hamasaki, P. Satir, Cloning and characterization of Kin5, a novel Tetrahymena ciliary kinesin II. *Cell Motil. Cytoskeleton* **58**, 1–9 (2004).
47. A. Awan, A. J. Bell, P. Satir, Kin5 knockdown in Tetrahymena thermophila using RNAi blocks cargo transport of Gef1. *PLoS One* **4**, e4873 (2009).
48. J. M. Brown, C. Marsala, R. Kosoy, J. Gaertig, Kinesin-II is preferentially targeted to assembling cilia and is required for ciliogenesis and normal cytokinesis in Tetrahymena. *Mol. Biol. Cell* **10**, 3081–3096 (1999).
49. D. Dave, D. Wloga, N. Sharma, J. Gaertig, DYF-1 Is required for assembly of the axoneme in *Tetrahymena thermophila*. *Eukaryot. Cell* **8**, 1397–1406 (2009).